Journal of the European Ceramic Society **19** (1999) 721–726

PII: S0955-2219(98)00303-3
0955-2219/99/$ - see front matter

Characterisation of $Zn_3(VO_4)_2$ Phases in V_2O_5-doped ZnO Varistors

Huey Hoon Hng* and Kevin M. Knowles

Department of Materials Science and Metallurgy, University of Cambridge, Pembroke Street, Cambridge, CB2 3QZ, UK

Abstract

Zinc oxide-rich ZnO–V_2O_5 (ZV), ZnO–V_2O_5–MnO_2 (ZVM) and ZnO–V_2O_5–Sb_2O_3 (ZVS) polycrystalline ceramics have been prepared for detailed microstructural and electrical characterisation. All samples exhibit non-linear current-voltage behaviour, with non-linear coefficients ranging from 5·0 for ZV to 16·7 for ZVM. The use of X-ray powder diffraction together with microstructural examination by transmission electron microscopy and a comparison of measured interplanar spacings with those quoted in the literature for α-, β- *and* γ-$Zn_3(VO_4)_2$, *has shown evidence for the formation of* β-$Zn_3(VO_4)_2$ *in ZV,* γ-$Zn_3(VO_4)_2$ *in ZVM and* α-$Zn_3(VO_4)_2$ *in ZVS. The* $Zn_3(VO_4)_2$ *phases are found to exist as smaller grains embedded in ZnO grains or residing at triple junctions. Electron diffraction suggests that* β-$Zn_3(VO_4)_2$ *has an orthorhombic A lattice, while* γ-$Zn_3(VO_4)_2$ *has a monoclinic* C *lattice.* © *1999 Elsevier Science Limited. All rights reserved*

Keywords: electron microscopy, microstructure-final, ZnO, varistors, $Zn_3(VO_4)_2$.

1 Introduction

Zinc oxide with several additives is widely used as a voltage regulator and surge protector because of its highly non-ohmic current-voltage characteristics.[1–4] It is generally accepted that these characteristics arise from modifications to the electrical characteristics of the zinc oxide grain boundaries caused by the segregation of large ionic additives such as Bi[1–5] Pr[6,7] and Ba.[8] Recent studies have shown that V_2O_5, which is a light-metal oxide, is a promising varistor former.[9–12] The ZnO-V_2O_5 ceramic system can be sintered at a relatively low temperature of about 900°C which makes it possible for a varistor to be cofired with a silver inner-electrode whose melting point is about 960°C. This is important for applications in multilayer chip components. Interestingly, no detailed transmission electron microscopy (TEM) microstructural studies have been undertaken in the ZnO–V_2O_5 system. Moreover, little information about the secondary phase $Zn_3(VO_4)_2$ known to form in this system can be found in the literature, other than that it occurs in three polymorphs—α, β and γ.[13] While the α polymorph is known to be orthorhombic,[14,15] no definitive crystal structures are quoted in the JCPDS files for the β- and γ-phases, although interplanar spacings and relative peak intensities are available.[13] To date, the effect of additives on the performance of ZnO–V_2O_5 varistor ceramics has received little attention—there is only a single report on the combined effects of low levels of Mn_3O_4, CoO, NiO, Nb_2O_5 and Na-glass in a multicomponent ZnO–V_2O_5 varistor.[12]

In this work, V_2O_5-based ZnO varistors containing MnO_2 and Sb_2O_3 were prepared and investigated. α-, β- and γ-$Zn_3(VO_4)_2$ phases were detected both by XRD and TEM in these samples. Lattice parameters and Bravais lattices for the β- and γ-$Zn_3(VO_4)_2$ phases are proposed on the basis of indexing diffraction patterns obtained from TEM which are also consistent with the XRD data reported by Brown and Hummel.[13]

2 Experimental Procedures

ZnO–0·25 mol% V_2O_5 (ZV), ZnO–0·25 mol% V_2O_5–1 mol% MnO_2 (ZVM) and ZnO–0·25 mol% V_2O_5–2 mol% Sb_2O_3 (ZVS) ceramic varistors were prepared from high purity oxide powder starting materials. The powder mixtures were ball-milled for 24 h using zirconia beads in deionised water. The mixtures were then dried and pressed into pellets. The pellets for ZV and ZVM were sintered in

*To whom correspondence should be addressed. Fax: +44-(0)1223-334-567; e-mail:hhh20@cus.cam.ac.uk

an atmosphere of ambient air for 4 h at 900°C and cooled at 5°C min^{-1}. ZVS pellets were not fully densified when sintered at 900°C, and a higher temperature of 1200°C had to be used in order to get a dense material.

The as-sintered specimens were lapped on both surfaces to ensure flat and parallel surfaces. They were coated with conductive silver paint on both surfaces, then heat cured to provide ohmic contacts. The current–voltage (I–V) characteristics were determined at room temperature using a variable dc power supply (Heathkit Model IP-17). X-ray analysis of the sintered samples were carried out using CuK_α radiation on a Philips PW1710 vertical powder diffractometer. Specimens for TEM were prepared using standard ion beam thinning methods and examined using a JEOL 2000FX at 200 kV.

3 Results

3.1 Current–voltage characteristics

The electrical properties of the V_2O_5-based ZnO materials were characterised by their current density-electric field (J–E) properties. The J–E curves for the samples are shown in Fig. 1. The corresponding parameters are summarised in Table 1. The results show that MnO_2 is effective in increasing further the varistor effect significantly, while Sb_2O_3 has at best a marginal effect. Furthermore, the resistivity is dramatically increased when MnO_2 is incorporated into the ZnO–V_2O_5 binary system.

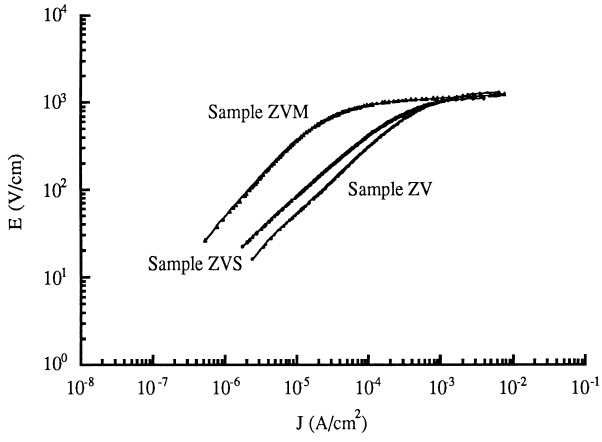

Fig. 1. The current density/electric field (J–E) curves for ZV, ZVM and ZVS.

3.2 X-ray diffraction results

The XRD traces for the three samples are shown in Fig. 2. β-$Zn_3(VO_4)_2$ and γ-$Zn_3(VO_4)_2$ phases are the only secondary phases detected in ZV and

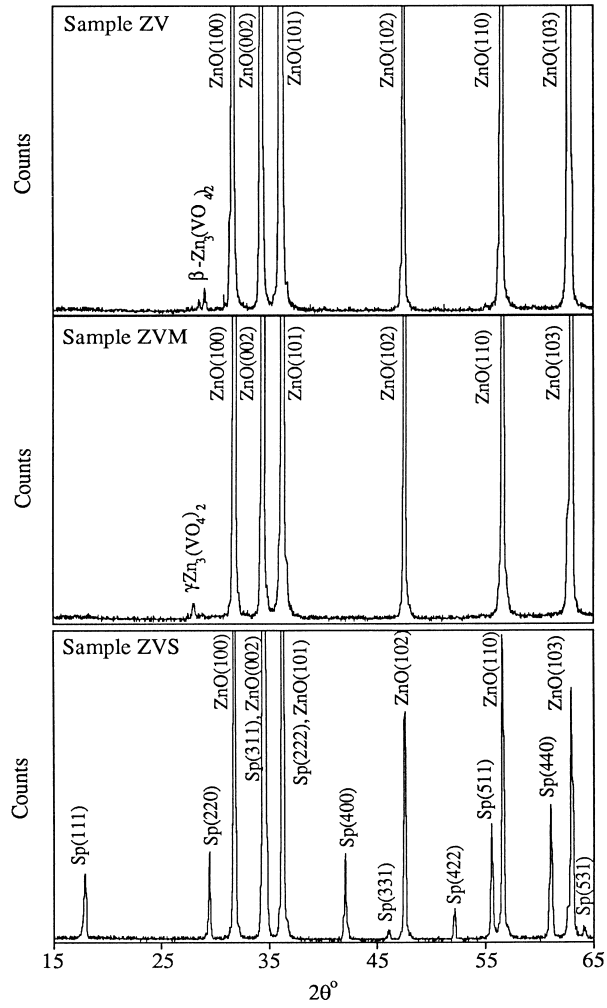

Fig. 2. X-ray diffraction patterns (CuK_α) for ZV, ZVM and ZVS.

Table 1. Summary of electrical results for ZnO–V_2O_5 varistor systems

Sample	*Composition*	*Sintering schedule*	*Resistivity in ohmic region ($M\Omega$ cm)*	*Non-linear coefficient, α*[a]	*Onset electric field (V cm^{-1})*[b]
ZV	ZnO–0·25 mol% V_2O_5	900°C for 4 h	3	5·0	1000
ZVM	ZnO–0·25 mol% V_2O_5–1 mol% MnO_2	900°C for 4 h	40	16·7	900
ZVS	ZnO–0·25 mol% V_2O_5–2 mol% Sb_2O_3	1200°C for 4 h	3	8·0	1000

[a] $\alpha = \frac{\log(J_2/J_1)}{\log(E_2/E_1)}$ where $J_1 = 0{\cdot}5$ mA cm^{-2} and $J_2 = 5$ mA cm^{-2}.

[b] The electric field at 1 mA cm^{-2}.

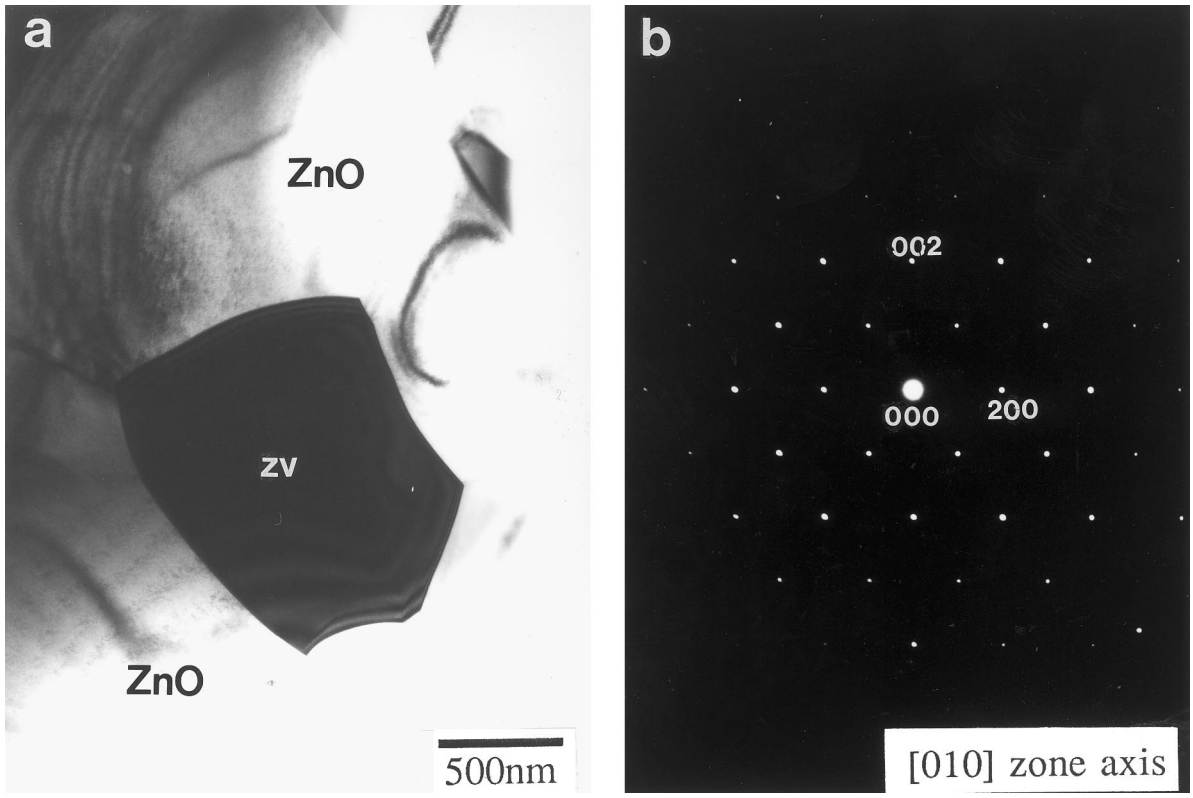

Fig. 3. (a) Bright-field image and (b) electron diffraction pattern of α-$Zn_3(VO_4)_2$ in ZVS. $Zn_3(VO_4)_2$ is denoted by zv in small letters.

ZVM, respectively, and only the spinel phase, $Zn_7Sb_2O_{12}$, is detected as a secondary phase in ZVS.

3.3 TEM observations

The samples all have a similar microstructure consisting mainly of ZnO grains and the minority $Zn_3(VO_4)_2$ phase. The identity of this minority phase was confirmed to be $Zn_3(VO_4)_2$ using energy dispersive X-ray analysis and from the magnitudes of the interplanar spacings seen in the electron diffraction patterns from this phase. The grains of $Zn_3(VO_4)_2$ phase are either embedded in the ZnO grains, or occur at triple points, as shown in Figs 3 and 4. $Zn_3(VO_4)_2$, which was not detected in ZVS using XRD, was however observed using TEM. This is likely be due to the fact that the amount of $Zn_3(VO_4)_2$ is too little to be detected using XRD. Moreover, the strongest peaks of $Zn_3(VO_4)_2$ polymorphs overlap with those of the major ZnO and spinel phases, making identification of a relatively small amount of $Zn_3(VO_4)_2$ difficult. The electron diffraction patterns (e.g. Fig. 3) obtained from the $Zn_3(VO_4)_2$ grains in ZVS can be indexed according to the α-$Zn_3(VO_4)_2$ polymorph, which has an orthorhombic structure (space group *Abam*), with $a = 8{\cdot}299$ Å, $b = 11{\cdot}5284$ Å, $c = 6{\cdot}1116$ Å (JCPDS 34-378). Electron diffraction patterns were also obtained for the $Zn_3(VO_4)_2$ phases in ZV and ZVM which XRD evidence suggested were the β and γ polymorphs, respectively. A systematic approach was used to deduce the crystal structures

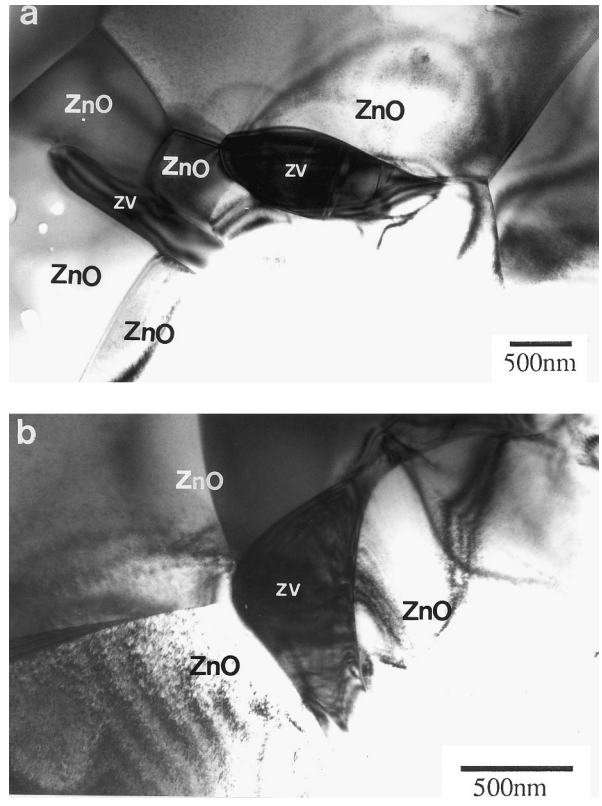

Fig. 4. Bright-field images of (a) β-$Zn_3(VO_4)_2$ and (b) γ-$Zn_3(VO_4)_2$ in ZV and ZVM, respectively, with zv denoting $Zn_3(VO_4)_2$.

for β- and γ-$Zn_3(VO_4)_2$ so that consistent indexing of these diffraction patterns could be achieved. The methodology used suggests that β-$Zn_3(VO_4)_2$ has an orthorhombic *A* lattice, with $a = 8{\cdot}34$ Å,

$b = 10{\cdot}68$ Å, and $c = 17{\cdot}0$ Å, while γ-$Zn_3(VO_4)_2$ has a monoclinic C lattice, with $a = 10{\cdot}40$ Å, $b = 8{\cdot}59$ Å, $c = 9{\cdot}44$ Å and $\beta = 98{\cdot}8°$. It is worth noting that the a and b lattice parameters for the β-$Zn_3(VO_4)_2$ are similar to those of α-$Zn_3(VO_4)_2$, and that the c of β-phase is nearly 3 times that of the α-phase. Hence, the β-phase can be viewed as a superlattice of the α-phase. Figures 5 and 6 show selected indexed electron diffraction patterns of β- and γ-$Zn_3(VO_4)_2$, respectively.

Spinel grains detected in ZVS were about 1 μm in size. The grains were usually located singly between ZnO grains. A typical example is shown in Fig. 7 of a bright-field image taken from ZVS. The spinel grains were mostly regular polyhedrally shaped, indicating that these grains have had plenty of time to adjust their shape to a near-equilibrium form while surrounded by a liquid phase.

4 Discussion

4.1 Current–voltage characteristics

The electrical conduction in ZnO–V_2O_5 binary ceramics can be rationalised in terms of a typical Schottky barrier controlled current behaviour, with the non-linearity characteristics occurring as a consequence of the existence of a grain boundary barrier layer.[9] In ZnO–Bi_2O_3, the addition of transition metal oxides significantly increases the non-linear behaviour. It has been postulated that transition metal oxides are involved in the formation of interfacial states and deep bulk traps at grain boundaries,[16] providing larger potential barriers to give better non-linear characteristics.[17] It is reasonable to infer that the same principle applies for the ZnO–V_2O_5 system, which therefore explains qualitatively the higher non-linear coefficient obtained for our sample containing MnO_2.

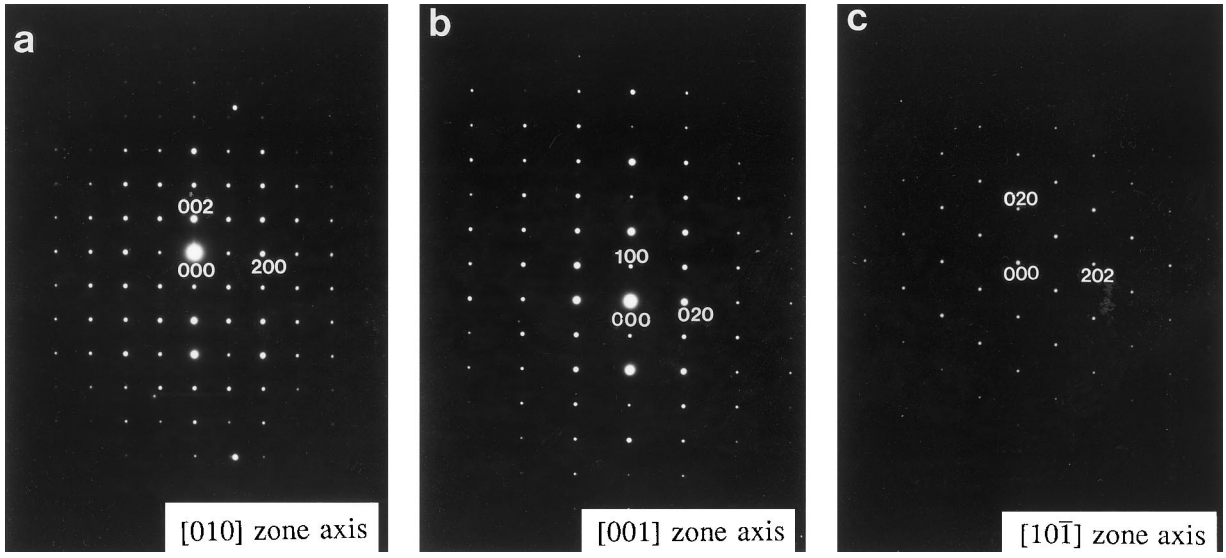

Fig. 5. Selected area diffraction patterns of β-$Zn_3(VO_4)_2$ in various zone axes: (a)[010], (b) [001] and (c) [10$\bar{1}$].

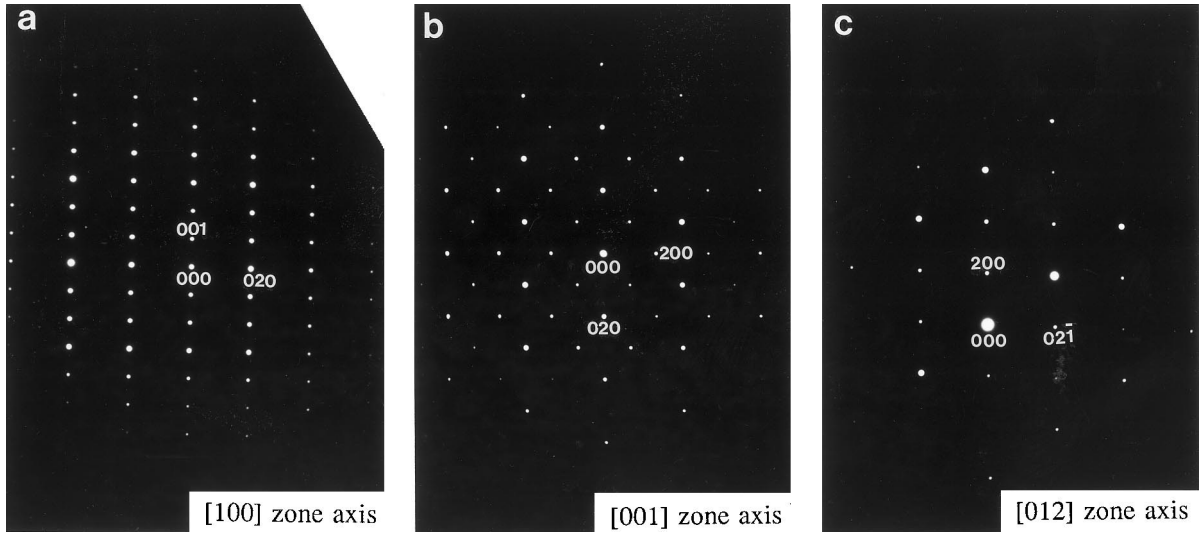

Fig. 6. Selected area diffraction patterns of γ-$Zn_3(VO_4)_2$ in various zone axes: (a)[100], (b) [001] and (c) [012].

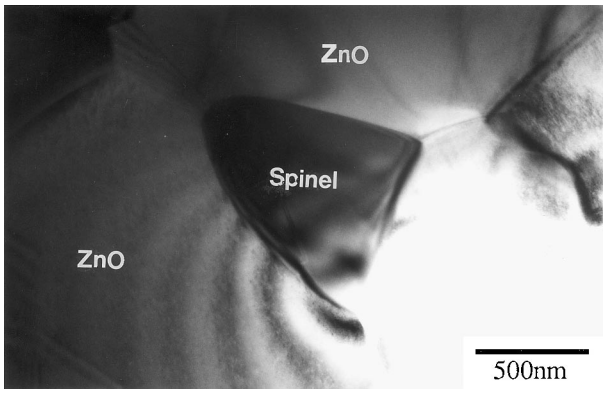

Fig. 7. A bright-field image of spinel phase between ZnO grains, taken from ZVS.

Sb_2O_3 is added to ZnO–Bi_2O_3 system for two reasons.[16] It suppresses grain growth by forming the spinel phase, $Zn_7Sb_2O_{12}$, and enhances the solubility of ions such as Zn in the Bi_2O_3-rich liquid phase. This latter role is very important for the defect distribution formed at the grain boundaries during cooling. However, in the ZnO–V_2O_5 system, the addition of Sb_2O_3 does not increase the non-linear coefficient significantly implying that it does not enhance the solubility of Zn in the vanadium-rich liquid phase.

4.2 $Zn_3(VO_4)_2$ phases

All three polymorphs of $Zn_3(VO_4)_2$ were detected in our samples, depending on the type of additives that were added into the system. α-$Zn_3(VO_4)_2$ is the stable room temperature phase and is found in ZVS, while the non-quenchable high-temperature β- and γ-phases are found in ZV and ZVM respectively. γ-$Zn_3(VO_4)_2$ is also detected in ZnO–V_2O_5 varistors containing trace amounts of Mn_3O_4, CoO, NiO, Nb_2O_5 and Na-glass.[12] These impurities presumably help to stabilise this high-temperature phase. In the case of Sb_2O_3 addition, the formation of the spinel phase might not be enough to stabilise the high temperature phase, enabling the α-phase to be formed instead. The formation of the β-phase in ZV suggest that the β-phase is not likely to be an impurity stabilised high temperature phase. $Zn_3(VO_4)_2$ phase is also reported by Tsai and Wu in binary ZnO–V_2O_5 ceramics.[9] However, they did not state which particular polymorph was formed.

High non-linear coefficients are obtained for V_2O_5-doped multicomponent ZnO varistor which have $Zn_3(VO_4)_2$ existing as the γ-phase.[12] In this work, the best non-linear characteristic is observed for ZVM which also contains γ-$Zn_3(VO_4)_2$. Thus, there is the implication of γ-$Zn_3(VO_4)_2$ in V_2O_5-doped zinc oxide ceramics may be a good indicator of desirable varistor behaviour, but further work is clearly required to identify those microstructural variables which give rise to optimum varistor behaviour in this family of materials.

5 Conclusions

V_2O_5 shows promise as a varistor former for ZnO-based varistors. Zinc oxide doped with V_2O_5 exhibits non-linear characteristics with non-linear coefficient comparable to that of the ZnO–Bi_2O_3 binary system. They can be fully densified at a lower sintering temperature (i.e. 900°C) compared to that needed for densifying Bi_2O_3-doped ZnO materials which is normally $\geq$ 1000°C. The highest non-linear coefficient of 16·7 is obtained for ZnO doped with 0·25 mol% V_2O_5 and 1 mol% MnO_2 (ZVM). α, β and γ–$Zn_3(VO_4)_2$ are detected in ZnO–V_2O_5–Sb_2O_3 (ZVS), ZnO–V_2O_5 (ZV) and ZnO–V_2O_5–MnO_2 (ZVM) varistor ceramics, respectively. Electron diffraction patterns suggest that β–$Zn_3(VO_4)_2$ has an orthorhombic A lattice, with $a = 8{\cdot}34$ Å, $b = 10{\cdot}68$ Å, and $c = 17{\cdot}0$ Å, while γ–$Zn_3(VO_4)_2$ has a monoclinic C lattice, $a = 10{\cdot}40$ Å, $b = 8{\cdot}59$ Å, $c = 9{\cdot}44$ Å and $\beta = 98{\cdot}8°$.

Acknowledgements

The authors would like to thank Professor A. H. Windle F.R.S. for the provision of laboratory facilities and Nanyang Technological University, Singapore for financial support for HHH.

References

1. Inada, M., Crystal phases of non-ohmic zinc oxide ceramics. *Jpn. J. Appl. Phys.*, 1978, **17**, 1–10.
2. Eda, K., Iga, A. and Matsuoka, M., Degradation mechanism of non-ohmic zinc oxide ceramics. *J. Appl. Phys.*, 1980, **51**, 2678–2684.
3. Levinson, L. M. and Philipp, H. R., Zinc oxide varistors—A review. *Am. Ceram. Soc. Bull.*, 1986, **65**, 639–646.
4. Gupta, T. K., Applications of zinc oxide varistors. *J. Am. Ceram. Soc.*, 1990, **73**, 1817–1840.
5. Wong, J., Sintering and varistor characteristics of ZnO–Bi_2O_3 ceramics. *J. Appl. Phys.*, 1980, **51**, 4453–4459.
6. Alles, A. B. and Burdick, V. L., The effect of liquid-phase sintering on the properties of Pr_6O_{11}-based varistors. *J. Appl. Phys.*, 1991, **70**, 6883–6890.
7. Alles, A. B., Puskas, R., Callahan, G. and Burdick, V. L., Compositional effects on the liquid-phase sintering of praseodymium oxide-doped zinc oxide varistors. *J. Am. Ceram. Soc.*, 1993, **76**, 2098–2102.
8. Matsuoka, M., Masuyama, T. and Lida, Y., Voltage non-linearity of zinc oxide ceramics doped with alkali earth metal oxide. *Jpn. J. Appl. Phys.*, 1969, **8**, 1275–1280.
9. Tsai, J. K. and Wu, T. B., Nonohmic characteristics of ZnO–V_2O_5 ceramics. *J. Appl. Phys.*, 1994, **76**, 4817–4822.
10. Tsai, J. K. and Wu, T. B., Microstructure and nonohmic properties of ZnO–V_2O_5 ceramics. *Jpn. J. Appl. Phys.*, 1995, **34**, 6452–6457.

11. Tsai, J. K. and Wu, T. B., Microstructure and nonohmic properties of binary ZnO–V_2O_5 ceramics sintered at 900°C. *Mat. Lett*., 1996, **26**, 199–203..
12. Chen, C. S., Kuo, C. T., Wu, T. B. and Lin, I. N., Microstructure and electrical properties of V_2O_5-based multicomponent ZnO varistors prepared by microwave sintering process. *Jpn. J. Appl. Phys*, 1997, **36**, 1169–1175.
13. Brown, J. J. and Hummel, F. A., Reactions between ZnO and selected oxides of elements of Groups IV and V. *Trans. Brit. Ceram. Soc*., 1965, **64**, 419–437.
14. Morris, M. C., McMurdie, H. F., Evans, E. H., Paretzkin, B., Parker, H. S., Pyrros, N. P. and Hubbard, C. R., Nat. Bur. Stand. (U.S.) Monogr. 25: Standard X-ray diffraction powder patterns, 1984, **20**, 111.
15. Gopal, R. and Calvo, C., Crystal structure of γ-$Zn_3(VO_4)_2$. *Canadian J. Chem*., 1971, **49**, 3056–3059.
16. Eda, K., Zinc oxide varistors. *IEEE Electrical Insulation Magazine*, 1989, **5**, 28–41.
17. Ezhilvalavan, S. and Kutty, T. R. N., Dependence of non-linearity coefficients on transition metal oxide concentration in simplified compositions of ZnO + Bi_2O_3 + MO varistor ceramics (M = Co or Mn). *J. Mater. Sci.: Mater. in Elec*., 1996, **7**, 137–148.